Available online at www.sciencedirect.com

SciVerse ScienceDirect

Ceramics International 39 (2013) 585–591

CERAMICS INTERNATIONAL

www.elsevier.com/locate/ceramint

High-frequency induction heated sintering of High-energy ball milled $TiC_{0.5}N_{0.5}$ powders and mechanical properties of the sintered products

Wonbaek Kim[a], Chang-Yul Suh[a], Ki-Min Roh[a], Jae-Won Lim[a], Sujeong Lee[a], Song-Lee Du[b], In-Jin Shon[b,*]

[a]*Minerals and Materials Processing Division, Korea Institute of Geoscience, Mining and Materials Resources, Daejeon, Republic of Korea*
[b]*Division of Advanced Materials Engineering and the Research Center of Advanced Materials Development, Engineering College, Chonbuk National University, 561-756, Republic of Korea*

Received 28 May 2012; received in revised form 10 June 2012; accepted 11 June 2012
Available online 5 July 2012

Abstract

Commercial $TiC_{0.5}N_{0.5}$ powders were high-energy ball milled for various durations and consolidated without binder using the high-frequency induction heated sintering method (HFIHS). The effect of milling on the sintering behavior, crystallite size and mechanical properties of TiCN powders were evaluated. A nanostructured dense TiCN compact with a relative density of up to 98% was readily obtained within 3 min. The ball milling effectively refined the crystallite structure of TiCN powders and facilitated the subsequent densification. The sinter-onset temperature was reduced appreciably by the prior milling for 10 h from 1170 °C to 820 °C. Accordingly, the relative density of TiCN compact increased as the milling time increases. The microhardness of sintered TiCN was linearly proportional to the density while its toughness did not show any correlation with the crystalline size or density. It is clearly demonstrated that a quick densification of nano-structured TiCN bulk materials to near theoretical density could be obtained by the combination of HFIHS and the preparatory high-energy ball milling processes.

Keywords: Nanomaterials; A. Sintering; C. Hardness; Fracture toughness

1. Introduction

TiCN is one of the promising ceramic materials, because it exhibits unusual combinations of physical and chemical properties such as high hardness, high melting point and excellent resistance to oxidation [1,2]. Industrial applications of the compound are in cutting tools and hard coatings. It is used extensively in cutting tool and abrasive materials in composite with a binder metal, such as Ni. The binder phase has inferior chemical characteristics compared to the carbide or nitride phase. Most notably, corrosion and oxidation occur preferentially in the binder phase [3]. Hence, the development of binderless TiCN is needed for water jet nozzle, mechanical seals and sliding parts due to their enhanced corrosion resistance and hardness.

Nanocrystalline materials have received much attention as advanced engineering materials with improved physical and mechanical properties. Since nanomaterials possess high strength, high hardness, relatively good ductility and toughness, undoubtedly, more attention has been paid to the application of nanomaterials [4–6]. In recent days, nanocrystalline powders have been developed by the thermochemical and thermomechanical process named the spray conversion process (SCP), co-precipitation and high energy milling [7–9]. However, the grain size in sintered materials becomes much larger than that in pre-sintered powders due to the rapid grain growth during a conventional sintering process. So, controlling grain growth during sintering is one of the keys to the commercial success of nanostructured materials. Unconventional

*Corresponding author. Tel.: +82 63 270 2381; fax: +82 63 270 2386.
E-mail address: ijshon@chonbuk.ac.kr (I.-J. Shon).

0272-8842/$36.00
http://dx.doi.org/10.1016/j.ceramint.2012.06.068

sintering techniques, including high-pressure densification, magnetic pulse compaction and shock densification, have been proposed to overcome the problem of grain growth [10]. However, these methods have failed to provide fast, reproducible techniques that yield large quantities of high density samples with nanostructured grains.

The high-frequency induction heated sintering (HFIHS) method recently emerged as an effective technique for sintering and consolidating high temperature materials [11,12]. HFIHS is similar to traditional hot-pressing, but the sample is heated by a induced electric current that flows through the sample and a die. This process increases the heating rate (up to 2000 °C/min) to a degree much higher than that of traditional hot-press sintering.

In this study, we investigated the binderless sintering behavior of TiCN using the HFIHS method. The effect of milling duration on the densification behavior, crystallite size and mechanical properties of TiCN powders were evaluated.

2. Experimental procedures

The TiCN powder used in this research was supplied by Treibacher Industrie AG (Germany). The average particle size was about 1.4 μm and the purity was 99%. The composition of C and N was 10.64 and 10.88 wt%, respectively. Oxygen was 0.24 wt%. The powder was first milled in a high-energy ball mill (Pulverisette-5 planetary mill) at 250 rpm for various time periods (0, 1, 4, and 10 h). Tungsten carbide balls (9 mm in diameter) were used in a sealed cylindrical stainless steel vial under an argon atmosphere. The weight ratio of balls-to-powder was 30:1. Milling resulted in a significant reduction in the particle size. The crystallite size of TiCN powders was calculated from the full width at half-maximum (FWHM) of the diffraction peak by Suryanarayana and Grant Norton's formula [13]

$$B_r(B_{crystalline}+B_{strain})\cos\theta = k\lambda/L+\eta\sin\theta \quad (1)$$

where B_r is the full width at half-maximum (FWHM) of the diffraction peak after instrumental correction; $B_{crystalline}$ and B_{strain} are FWHM caused by small grain size and internal stress, respectively; k is a constant (with a value of 0.9); λ is wavelength of the X-ray radiation; L and η are the grain size and internal strain, respectively; and θ is the Bragg angle. The parameters B and B_r follow Cauchy's form with the relationship: $B=B_r+B_s$, where B and B_s are the FWHM of the broadened Bragg peaks and the standard sample's Bragg peaks, respectively.

The powders were placed in a graphite die (outside diameter 45 mm, inside diameter 20 mm, height 40 mm) and introduced into the high-frequency induction heated sintering (HFIHS) apparatus shown schematically in Fig. 1. The HFIHS apparatus includes a 15 kW power supply which provides an induced current through the sample under 50 kN uniaxial load. The system was first evacuated and a uniaxial pressure of 80 MPa was applied. An induced current was then activated and maintained

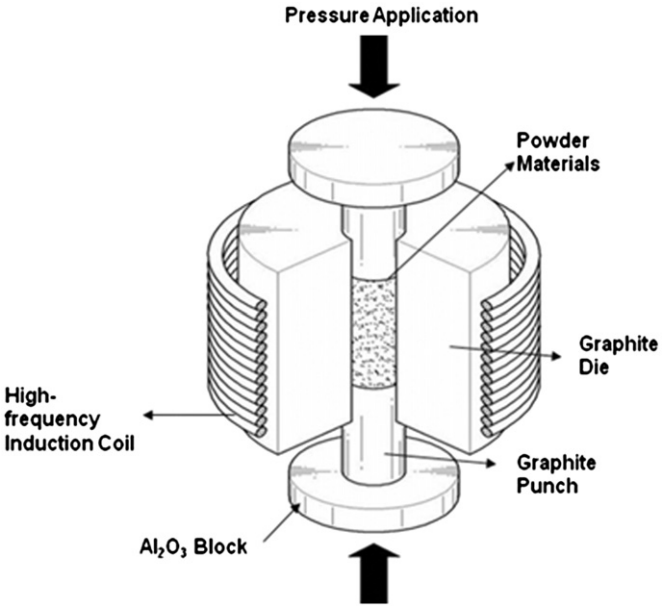

Fig. 1. Schematic diagram of the apparatus for the high-frequency induction heated sintering (HFIHS).

until the densification rate became negligible according to the real-time output of the sample shrinkage. The shrinkage was measured by a linear gage which shows the vertical displacement. Temperatures were measured by a pyrometer focused on the surface of the graphite die. At the end of the process, the induced current was turned off and the sample cooled to room temperature. The process was carried out under a vacuum of 4×10^{-2} Torr (5.33 Pa).

The relative density of sintered sample was measured by the Archimedes method. Microstructural information was obtained from the surface of the samples, which were polished and etched using Murakami's reagent (10 g potassium ferricyanide, 10 g NaOH, and 100 mL water) for 1–2 min at room temperature. Compositional and microstructural analyses of the products were carried out by X-ray diffraction (XRD), scanning electron microscopy (SEM) with energy dispersive spectroscopy (EDS) and field emission scanning electron microscope (FE-SEM). Vickers hardness was measured at a load of 10 kg_f and a dwell time of 15 s.

3. Results and discussion

3.1. Effect of milling on crystallite size

The high-energy milling refined the microstructure of TiCN particles. Fig. 2(a–d) shows X-ray diffraction patterns of the TiCN powders after milling for 1–10 h. The broadening of TiCN peaks due to crystallite refinement is evident after milling for 1 h, and it continuously broadened during the prolonged milling. The milling process is known to introduce impurities from the ball and/or container. However, in this study, peaks other than TiCN were not identified. SEM images of Fig. 3(a–d) shows the particle size reduction occurred during the high-energy milling process. The TiCN

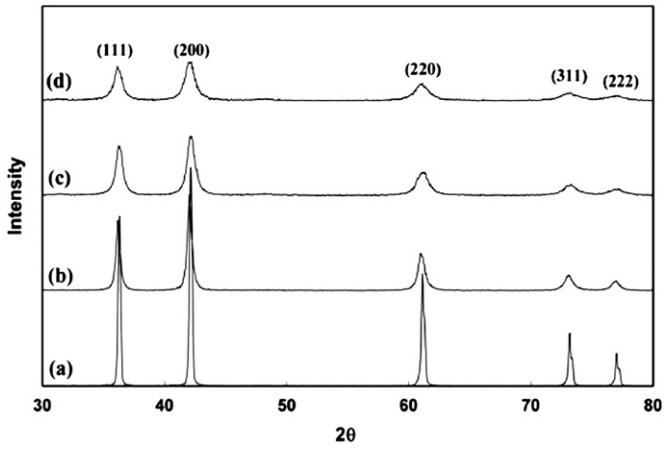

Fig. 2. X-ray diffraction patterns of the TiCN powder after high-energy milling for various durations: (a) as-received (b) milled for 1 h, (c) milled for 4 h, and (d) milled for 10 h.

crystallite size by Suryanarayana and Grant Norton's formula was reduced to 75, 18, and 9 nm by milling for 1, 4, 10 h, respectively (Table 1). The crystallite size reduction was most pronounced during the 1st hour of milling.

The milling increased the specific surface area of TiCN powders as manifested by the BET result (Table 1). The specific surface area of the milled powders increased almost linearly with the milling time. The particle size can be estimated as D (diameter)$=6/(\rho * S)$. Here, ρ is the density and S is the BET surface area. The milling usually produces clusters of particles. Therefore, it would be an exception if the sizes calculated by both means match exactly. This may be the reason why the particle size measured by BET was much larger than that measured by XRD. In any case, it is obvious that the milling effectively refined the microstructure of TiCN raw powders which should help the densification process thereafter (Table 2).

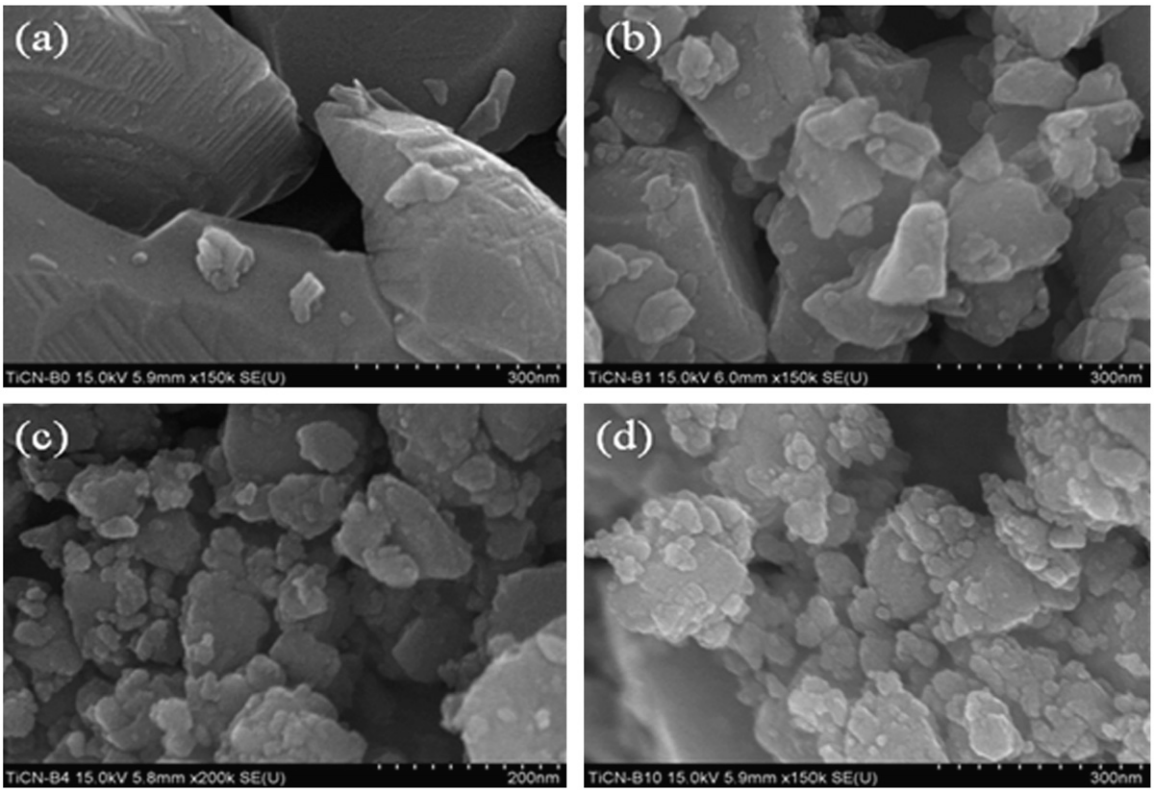

Fig. 3. SEM microgrphss of TiCN powders after milling for various durations: (a) as received, (b) 1 h, (c) 4 h, and (d) 10 h.

Table 1
Physical properties of TiCN powders after milling.

Sample	BET (m^2/g)	Crystallite size by XRD (nm)	Particle size by BET (nm)	Oxygen (wt%)
As received	1.24	231	936	0.52
Milled for 1 h	6.35	80	182	1.61
Milled for 4 h	12.75	19	91	2.86
Milled for 10 h	14.33	9	81	3.77

Table 2
Mechanical properties of sintered TiCN compacts.

Sample	Relative density (%)	Crystallite size (nm)	Vickers hardness ($kg \cdot mm^{-2}$)	Toughness ($Mpa \cdot m^{1/2}$)
As received	77	227	410	–
Milled for 1 h	89	201	1300	6.6
Milled for 4 h	95	196	1580	6.5
Milled for 10 h	99	158	1910	6.7

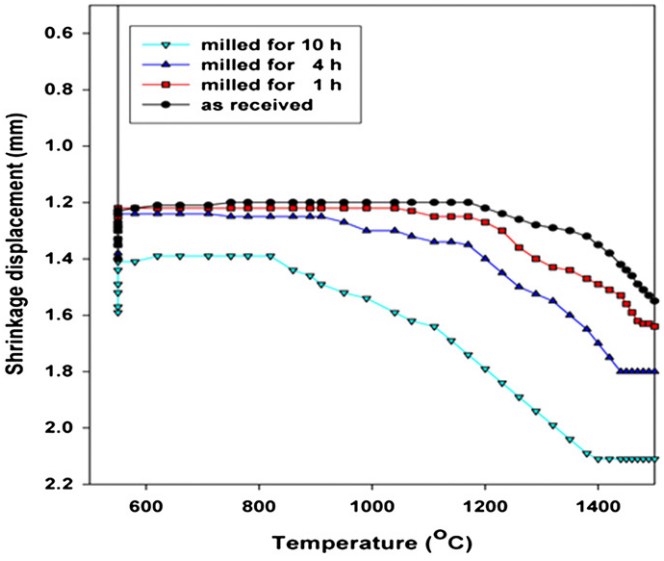

Fig. 4. Shrinkage displacement-temperature curve during the high-frequency induction heated sintering of TiCN powders milled for various durations.

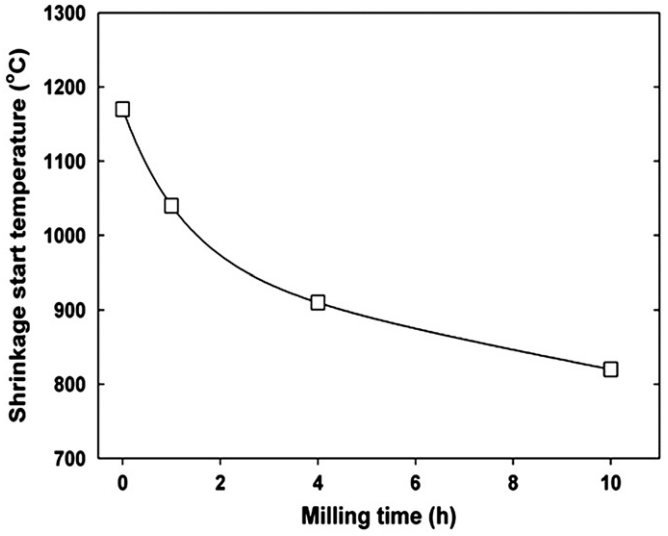

Fig. 5. The effect of milling time on the onset of shrinkage-start temperature.

3.2. Effect of milling on sintering-start temperature

The shrinkage displacement-time (temperature) curve provides an important information on the consolidation behavior. Fig. 4 shows the shrinkage record of TiCN compacts under the applied pressure of 80 MPa. In all cases, there was a brief thermal expansion period as soon as the induced current was applied. After the initial expansion, the displacement shows a plateau region for about 40–60 s before the start of the continuous shrinkage depending on the milling conditions. The amount of shrinkage displacement, which should be indication of densification degree, increases with the milling time. Fig. 5 shows the variation of the shrinkage-start temperature for TiCN compacts milled for different durations. It is clearly seen that the shrinkage-start temperature decreases as the milling time increases. The as-received TiCN powders started to shrink after about 80 s which corresponds to 1170 °C. In contrast, TiCN powders milled for 10 h start to shrink at a much lower temperature of 820 °C. This demonstrates the effectiveness of prior-milling on the densification of TiCN powders.

3.3. Microstructure of TiCN compact

Fig. 6 shows the X-ray diffraction patterns of milled TiCN powders after sintering. All peaks are TiCN and

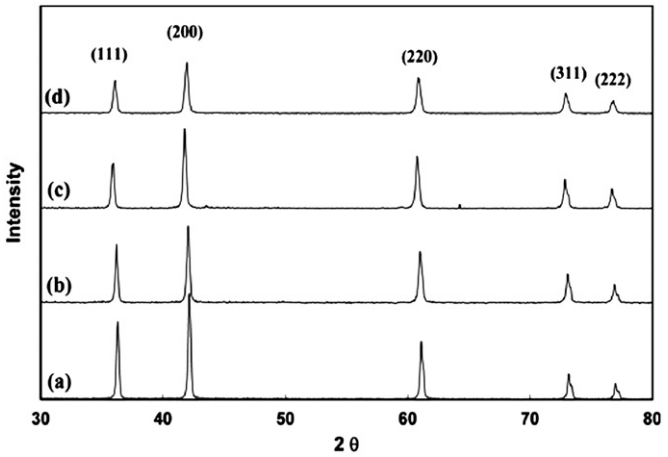

Fig. 6. X-ray diffraction patterns of the sintered compact using TiCN powders after milling for various durations: (a) as-received (b) milled for 1 h, (c) milled for 4 h, and (d) milled for 10 h.

their peak broadening was seen to reduce suggesting that there would be some grain growth during sintering. As can be anticipated from the shrinkage displacement result, the high-energy ball milling enhanced the densification significantly. Nevertheless, it is also necessary to mention that one of the reasons for the enhanced densification may be that the clusters of as-received powders were broken effectively for a denser compaction. Fig. 7(a–d) shows SEM images of polished surface of the sintered TiCN

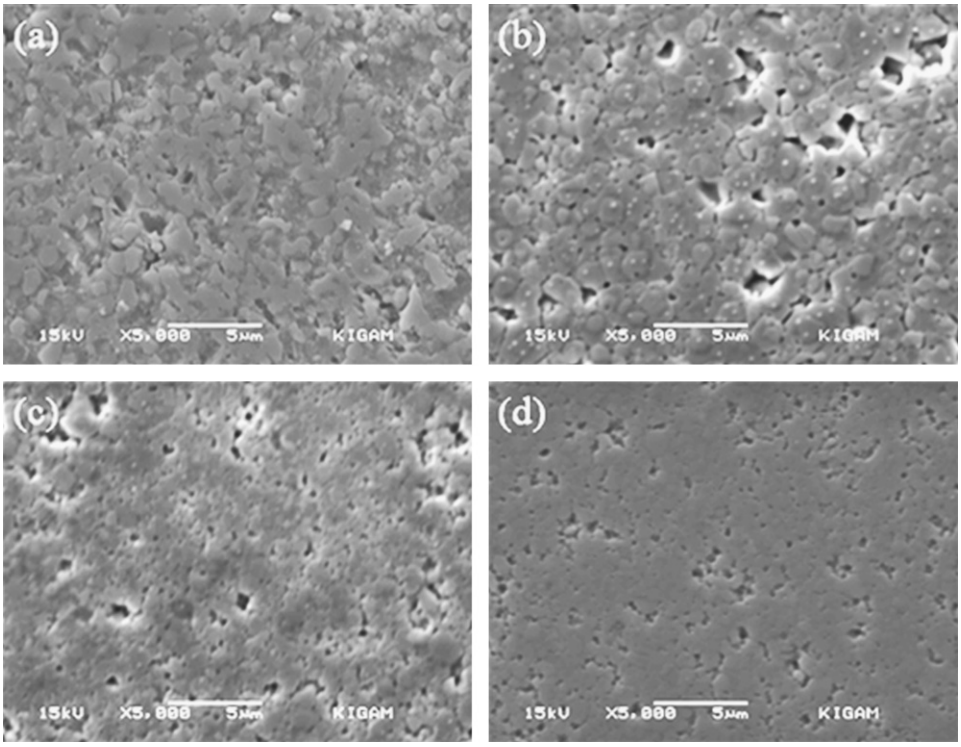

Fig. 7. SEM micrographs showing the polished and etched surface of TiCN compacts: (a) as-received (b) milled for 1 h, (c) milled for 4 h, and (d) milled for 10 h.

compact. The reduction of pore volume with milling time is obvious. It became dense and had more refined microstructure as the milling time increases. The microstructural refinement can be better recognized on the fracture surface. Fig. 8(a–d) shows the SEM micrographs showing the intergranular-type fracture surface of sintered TiCN compact. It is obvious that the crystallite size becomes finer as the milling time increases.

As previously presented, milling effectively refined microstructure of TiCN powders and sintered compacts. Fig. 9 shows the effect of milling on the crystallite size for milled powders and sintered compacts. The crystallite size is seen to decrease significantly by milling. It became larger during sintering suggesting that some grain growth occurred. Nevertheless, the average crystallite size of the sintered TiCN is not greatly larger than that of the milled powders and is still in the nano-scale realm. The retention of the nanoscale crystallite size might be attributed to the high heating rate and the relatively short exposure time of the powders to high temperature in HFIHS.

The role of the current (resistive or inductive) in sintering has been the focus of several attempts aimed at providing an explanation of the observed enhancement of sintering and the improved characteristics of the products. The role played by the current has been variously interpreted, the effect being explained in terms of a fast heating rate due to Joule heating, the presence of a plasma in pores separating powder particles, and the intrinsic contribution of the current to mass transport [14–17].

3.4. Mechanical properties of TiCN compact

Vicker hardness and fracture toughness was measured to evaluate the mechanical properties of TiCN compact. Vickers hardness measurements were performed on polished sections of the TiCN samples using a 10 kg_f load and 15 s dwell time. Indentations with large enough loads produced radial cracks emanating from the corners of the indent. The lengths of these cracks permit estimation of the fracture toughness of the materials by means of the expression [18]

$$K_{IC} = 0.203(c/a)^{-3/2} H_v a^{1/2} \quad (2)$$

where c is the trace length of the crack measured from the center of the indentation, a is one half of the average length of the two indent diagonals, and H_v is the hardness.

The hardness of sintered TiCN increased as the milling time increased. This effect may be attributed to the refined microstructure and/or higher density. One can expect that the refinement of the crystalline size by milling would increase the hardness. In this case, however, the crystallite size effect on the hardness may not be evaluated because of two reasons. One is that the variation of the crystallite size is not large enough considering the possible errors in the crystallite size measurement by XRD. Another, more importantly, is that the difference of density between samples is too large to consider the crystallite size effect properly. As a matter of fact, the hardness was more closely related to the relative density of the compact. Fig. 10 shows the effect of density on the hardness and fracture toughness of TiCN

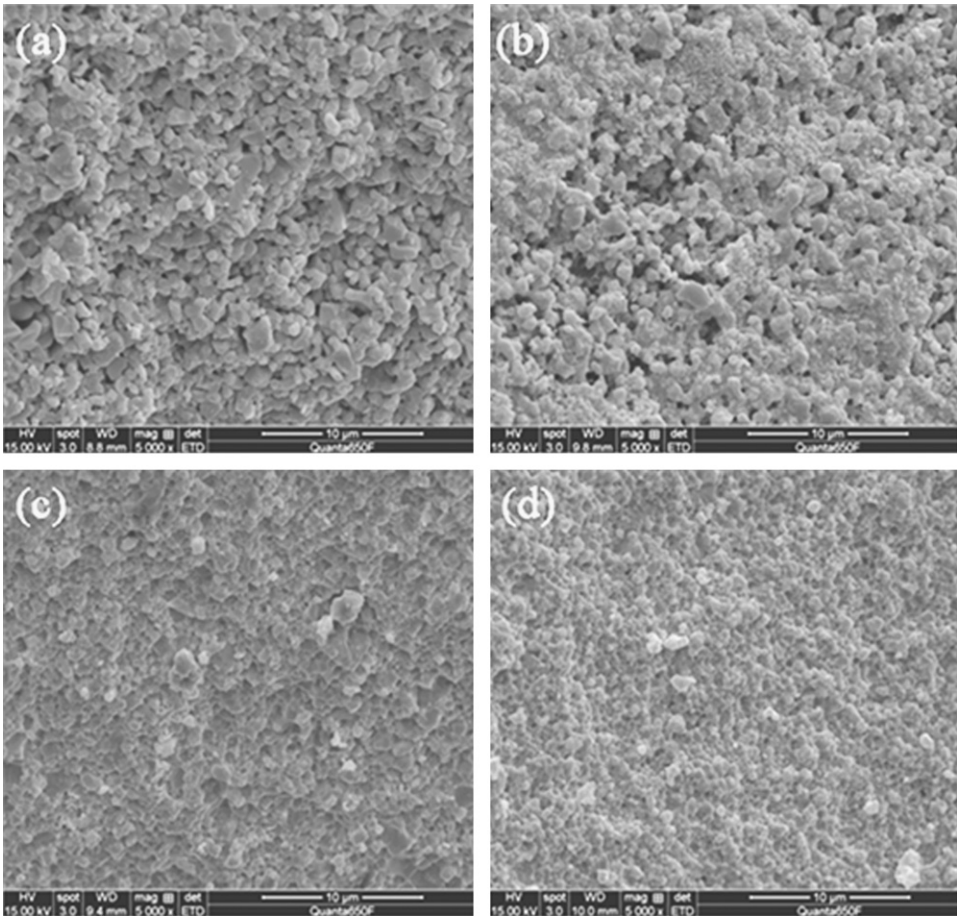

Fig. 8. SEM micrographs showing the fracture surface of TiCN compacts: (a) as-received (b) milled for 1 h, (c) milled for 4 h, and (d) milled for 10 h.

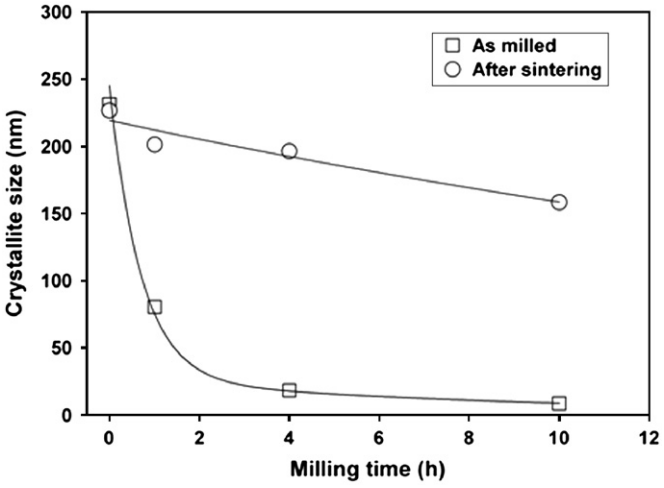

Fig. 9. The effect of milling time on the crystalline size of TiCN powders and sintered compacts.

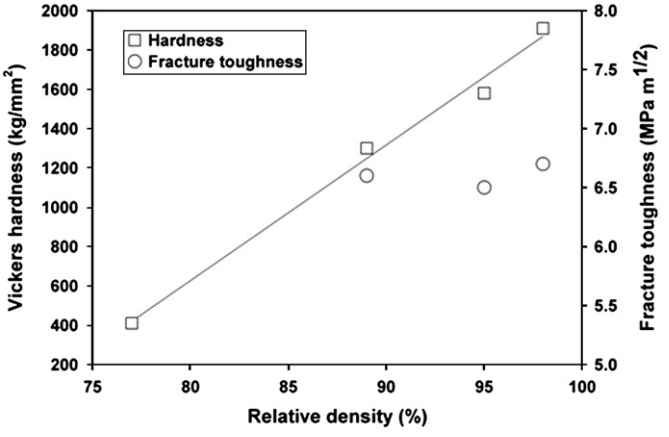

Fig. 10. The effect of crystallite size on microhardness and toughness of sintered TiCN compacts.

compacts. A linear relationship between the density and hardness is evident. The dependence of hardness on density gives, $H_v = 68.986 \times$ Relative density(%) $- 4891$ with a correlation coefficient R, of 0.99. However, the fracture toughness of TiCN compact did not show any dependence on crystallite size or density. It was 6.6 MPa $m^{1/2}$, 6.5 MPa $m^{1/2}$, and 6.7 MPa $m^{1/2}$, for sintered compacts milled for 1 h, 4 h, and 10 h, respectively.

4. Summary

Commercial $TiC_{0.5}N_{0.5}$ powders were high-energy ball milled for various durations and consolidated without

binder using the high-frequency induction heated sintering method (HFIHS). The ball milling substantially refined the crystallite structure of TiCN powders and facilitated the subsequent densification process. The consolidation temperature of TiCN powders was reduced by milling for 10 h from 1170 °C to 820 °C. The milling for 10 h reduced the crystallite size from 231 nm to 9 nm. The rapid consolidation of the HFIHS process retained the fine microstructure after sintering with decent mechanical properties. The microhardness of sintered TiCN was linearly proportional to the relative density while its fracture toughness did not reveal any correlation with density or crystallite size.

Acknowledgments

This study was supported by a grant from basic research project of Korea Institute of Geoscience and Mineral Resources and by the Human Resources Development of the Korea Institute of Energy Technology Evaluation and Planning (KETEP) grant funded by the Korea government Ministry of Knowledge Economy (No. 20114030200060).

References

[1] B. Gomez, A. Jimenez, E. Gordo, Oxidation and tribological behavior of an Fe-based MMC reinforced with TiCN particles, International Journal of Refractory Metals and Hard Materials 27 (2009) 336–360.

[2] D. Mari, S. Bologini, T. Viatte, Study of the mechanical properties of TiCN–WC–Co hardmetals by the interpretation of internal friction spectra, International Journal of Refractory Metals and Hard Materials 19 (2001) 257–265.

[3] S. Imasato, K. Tokumoto, T. Kitada, S. Sakaguchi, Properties of ultra-fine grain binderless cemented carbide RCCFN, International Journal of Refractory Metals and Hard Materials 13 (1995) 305–312.

[4] L. Fu, L.H. Cao, Y.S. Fan, Two-step synthesis of nanostructured tungsten carbide-cobalt powders, Scripta Materialia 44 (2001) 1061–1065.

[5] K. Niihara, A. Nikahira, Advanced Structural Inorganic Composite, Elsevier Scientific Publishing Co., Trieste, Italy, 1990, pp. 637-64.

[6] S. Berger, R. Porat, R. Rosen, Nanocrystalline materials: a study of WC-based hard matals, Progress in Materials 42 (1997) 311–322.

[7] Z. Fang, J.W. Eason, Study of nanostructured WC–Co composites, International Journal of Refractory Metals and Hard Materials 13 (1995) 297–302.

[8] I.Y. Ko, J.H. Park, K.S. Nam, I.J. Shon, Rapid consolidation of nanocrystalline $NbSi_2$–Si_3N_4 composites by pulsed current activated combustion synthesis, Metals and Materials International 16 (2010) 393–398.

[9] I.J. Shon, S.L. Du, I.Y. Ko, J.M. Doh, J.K. Yoon, J.H. Park, Effect of Fe_2O_3 on properties and densification of 8 YSZ by pulsed current activated sintering, Electronic Materials Letters 7 (2011) 133–137.

[10] S.C. Liao, W.E. Mayo, K.D. Pae, Theory of high pressure/low temperature sintering of bulk nanocrystalline TiO_2, Acta Materialia 45 (1997) 4027–4040.

[11] I.Y. Ko, S.M. Chae, I.J. Shon, The effect of rapid consolidation of nanostructured $MoSi_2$-SiC composite on its mechanical properties, Korean Journal of Metals and Materials 48 (2010) 417–423.

[12] I.Y. Ko, J.H. Park, J.K. Yoon, J.M. Doh, I.J. Shon, Properties and synthesis of dense nanostructured VSi_2–SiC by high-frequency induction heated combustion, Metals and Materials International 16 (2010) 219–223.

[13] C. Suryanarayana, M.Grant Norton, X-ray Diffraction A Practical Approach, Plenum Press, New York, 1998.

[14] Z. Shen, M. Johnsson, Z. Zhao, M. Nygren, Spark Plasma Sintering of Alumina, Journal of the American Ceramic Society 85 (2002) 1921–1927.

[15] J.E. Garay, U. Anselmi-Tamburini, Z.A. Munir, S.C. Glade, P. Asoka- Kumar, Electric current enhanced defect mobility in Ni_3Ti intermetallics, Applied Physics Letters 85 (2004) 573–575.

[16] J.R. Friedman, J.E. Garay, U. Anselmi-Tamburini, Z.A. Munir, Modified interfacial reactions in Ag–Zn multilayers under the influence of high DC currents, Intermetallics 12 (2004) 589–597.

[17] J.E. Garay, U. Anselmi-Tamburini, Z.A. Munir, Enhanced growth of intermetallic phases in the Ni–Ti system by current effects, Acta Materialia 51 (2003) 4487–4495.

[18] K. Niihara, R. Morena, D.P.H. Hasselman, Evaluation of KIC of brittle solids by the indentation method with low crack-to-indent ratios, Journal of Materials Science Letters 1 (1982) 12–16.